Charge transport in amorphous InGaZnO thin-film transistors

W. Chr. Germs,[1] W. H. Adriaans,[1] A. K. Tripathi,[2] W. S. C. Roelofs,[1] B. Cobb,[2] R. A. J. Janssen,[2] G. H. Gelinck,[2] and M. Kemerink[1,*]

[1]*Department of Applied Physics, Eindhoven University of Technology, P. O. Box 513, 5600 MB Eindhoven, The Netherlands*

[2]*Holst Centre/TNO, High Tech Campus 31, 5656 AE Eindhoven, The Netherlands*

(Received 13 August 2012; revised manuscript received 8 October 2012; published 26 October 2012)

We investigate the mechanism of charge transport in indium gallium zinc oxide (a-IGZO), an amorphous metal-oxide semiconductor. We measured the field-effect mobility and the Seebeck coefficient ($S = \Delta V/\Delta T$) of a-IGZO in thin-film transistors as a function of charge-carrier density for different temperatures. Using these transistors, we further employed a scanning Kelvin probe-based technique to determine the density of states of a-IGZO that is used as the basis for the modeling. After comparing two commonly used models, the band transport percolation model and a mobility edge model, we find that both cannot describe the full properties of the charge transport in the a-IGZO semiconductor. We, therefore, propose a model that extends the mobility edge model to allow for variable range hopping below the mobility edge. The extended mobility edge model gives a superior description of the experimental results. We show that the charge transport is dominated by variable range hopping below, rather than by bandlike transport above the mobility edge.

DOI: 10.1103/PhysRevB.86.155319 PACS number(s): 73.61.Jc, 73.50.Lw, 71.23.An, 81.05.Gc

I. INTRODUCTION

Amorphous oxide semiconductors (AOSs) are of interest for their use as transparent and flexible backplanes and electrodes in, among others, displays and photovoltaic cells. Consequently, the charge transport in AOSs received considerable attention. In recent literature, two types of charge transport models can be found for AOSs: a band transport percolation model[1–3,6] and the mobility edge (ME) model[4,5] also known as the multiple trapping and release model. This situation is particularly unsatisfactory as these models are based on fundamentally different physical assumptions regarding the nature of the charge transport in AOSs. In this paper, we confront the two types of models with an extensive set of thermoelectric measurements obtained on amorphous InGaZnO (a-IGZO) field-effect transistors. a-IGZO was introduced by Nomura *et al.*[6] in 2004 and can reach charge-carrier mobilities in excess of 10 $cm^2\ V^{-1}\ s^{-1}$. In the last decade, several papers were published on the nature of the charge transport in a-IGZO; a recent review can be found in Ref. 7.

The percolation[1] model assumes charge transport to take place in a conduction band with a square-root energy dependence of the densities of states (DOS). Furthermore, the presence of a Gaussian distribution of potential barriers is assumed that limit the contribution of low-energy band states to the conductivity. The charge transport is then described in a manner that is similar to the standard Boltzmann transport formalism but with the addition of the barriers. For the remainder of this paper, we refer to this model as the Kamiya-Nomura model.

By investigating the optical response in capacitance-voltage characteristics, Park *et al.*[8] and Jeon *et al.*[9] extracted a different DOS for a-IGZO, consisting of an exponential tail. When the exponential tails are assumed to be trap states that do not contribute to the conduction, this gives rise to a charge transport description in terms of a ME model. In a ME model, the Fermi level lies in a tail of localized states, and transport is assumed to take place by charges that are thermally excited over a mobility edge that separates localized and delocalized or bandlike states. However, at low temperatures, the charge transport in such systems is expected to occur via hopping-type processes.[10] Only at sufficiently high temperatures is transport dominated by the mobility edge. So far, hopping has been assumed to be irrelevant in a-IGZO because of the observation of a well-developed Hall effect, which implies the occupation of bandlike states.[3,7] Therefore, we extend the ME model to allow for variable range hopping (VRH) in the localized states in addition to the bandlike transport above the mobility edge.

Here, we compare the Kamiya-Nomura model to the extended mobility edge (eME) model. Both the Kamiya-Nomura and the eME model were used to simultaneously describe measured charge-carrier mobilities and Seebeck coefficients ($S = \Delta V/\Delta T$) as a function of charge-carrier density and temperature. In order to constrain the degrees of freedom in the fitting procedure, we used a scanning Kelvin probe microscopy- (SKPM)-based technique to determine the density of states on the same type of device.[11] We find that, in our devices, the charge transport can only be consistently described by the eME model and that, over the entire investigated temperature and density range, the transport is dominated by hopping processes.

In the next section, we give a description of the device fabrication, followed by a description of the thermoelectric measurement procedures in Sec. III. In Sec. IV, we describe the theoretical framework used to interpret the experimental results in Sec. V. Section VI summarizes our findings.

II. DEVICE PREPARATION

Thin-film transistors (TFTs) were prepared using a highly doped Si substrate as the gate electrode and 200 nm of thermally grown SiO_2 as the gate dielectric. This bottom contact blanket gate approach allows for excellent heat transfer through the substrate and the device. Source and drain electrodes consisted of a 5-nm titanium adhesion layer followed by 25 nm of gold and were defined using UV lithography. The channel length and width of the used devices were 500 and 100 μm, respectively. A 10-nm-thick a-IGZO layer was then

deposited via rf sputtering from an Advanced Nano Products IGZO target (2:2:1 In:Ga:Zn metal ratio, leading to a 1:1:1 Ga_2O_3:In_2O_3:ZnO oxide ratio) at 10^{-3} mbar pressure and room temperature. A partial pressure of oxygen in argon of 2% was maintained throughout the deposition in the sputter chamber. This is the same procedure as followed in Ref. 12, apart from the annealing step, which was performed at 400 °C for 20 min in air.

III. THERMOELECTRIC MEASUREMENT PROCEDURES

When a temperature difference ΔT is applied to a material, it, in general, causes a thermovoltage ΔV. The Seebeck coefficient is equal to the ratio between the thermovoltage and the temperature $S = \Delta V/\Delta T$.[13] We will use Seebeck coefficient measurements to investigate different charge transport models.

The thermovoltage is measured using a Keithley 4200 SCS. The measurements are performed in a Janis ST-500 probe station where, under high-vacuum conditions ($<10^{-5}$ mbar), the temperature of the sample holder and the TFT can be varied. Two Peltier elements are placed on the sample holder to apply a temperature gradient across the TFT channel. Figure 1(a) schematically shows the sample holder. On top of the sample, above each Peltier element, a Si-diode temperature sensor is placed. The TFT is positioned between the two Peltier elements. The high thermal conductivity of the Si common gate electrode determines the shape of the temperature profile of the whole sample. The temperature gradient is assumed to be constant between the Peltier elements as depicted in Fig. 1(b). The temperature difference can then be calculated from the temperature difference between the Peltier elements ΔT_P, the distance between the Peltier elements x_P, and the distance between the source (S) and the drain (D) electrodes x_{SD}, $\Delta T = \Delta T_P \times x_{SD}/x_P$. From finite-element calculations, we determined the range of temperature differences between the Peltier elements at which the assumed constant temperature gradient in Fig 1(b) was still a good approximation, and we found that, for a ΔT_P equal to 35 K over a distance of $x_P = 4$ mm, the error in ΔT is smaller than 10%. The validity of the assumption is further verified by measuring the thermovoltage ΔV for different ΔT's as shown in Fig. 1(c). The Seebeck coefficient has been determined from the gradient of a linear fit through these measurement points. By using the gradient, we reduce both systematic and random errors.

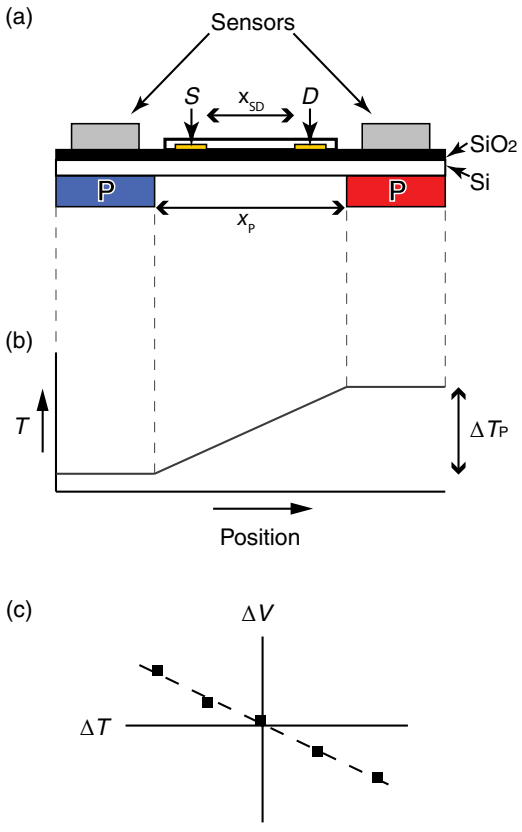

FIG. 1. (Color online) (a) A drawing representing the sample and sample holder, with P being the Peltier elements and S (D) being the source (drain) electrodes. (b) The typical temperature vs position for the sample in (a). (c) Representation of measured thermovoltage vs temperature difference. The derivative of the fitted line equals the Seebeck coefficient S.

The above procedure is followed for each different gate bias and temperature.

By switching off the Peltier elements, the same setup can be used to measure transfer and output curves just before or after a Seebeck measurement. From the transfer curves in the linear regime ($V_D = 2$ V), the temperature- and gate-voltage-dependent mobilities are calculated as

$$\mu = \frac{L}{CWV_D}\frac{\partial I_{SD}}{\partial V_G}, \tag{1}$$

with L as the channel length, W as the channel width, and C as the capacitance per unit area.

IV. THEORY

A. The Kamiya-Nomura model

The Kamiya-Nomura model is very similar to the standard Boltzmann transport formalism, which can be found in, for example, Ref. 13. In addition to the usual description of band transport, the model assumes a Gaussian distribution of potential barriers in the band. These barriers are attributed to the Ga^{3+} and Zn^{2+} ions.[3,7] The potential barriers can hinder conduction and, thereby, can reduce the contribution of charge carriers in low-energy states. A cartoon to visualize the model is given in Fig. 2. A typical conduction band is shown in

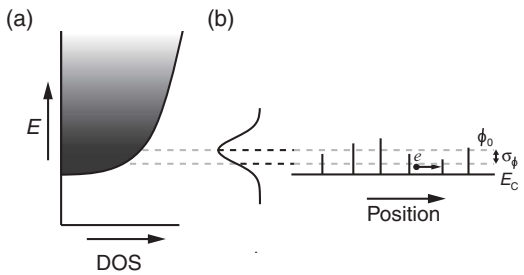

FIG. 2. (a) The conduction band as a function of energy. (b) The Gaussian represents the position of the distribution of potential barriers in the conduction band. The cartoon at the right shows a low-energy electron in the conduction band that is "trapped" between two potential barriers.

Fig. 2(a). The Gaussian in Fig. 2(b) represents a distribution of potential barriers. To the right of the Gaussian, a low-energy electron in the conduction band is shown between the barriers; at higher energies, electrons become increasingly less hindered by the barriers. The mathematical description of the model is based on the paper by Adler *et al.*[14] An extra term $p(E)$ is added to the transport equation, representing a Gaussian distribution of barriers. The conductivity is given by[1]

$$\sigma_{KN} = -\frac{e^2}{m_e^*}\int_{E_C}^{\infty} p(E)\tau(E)v_z(E)\frac{\partial f_{FD}}{\partial v_z}D_C(E)dE, \quad (2)$$

with e as the elementary charge, m_e^* as the effective mass, E_C as the conduction-band onset, τ as the relaxation time, v_z as the electron velocity, f_{FD} as the Fermi-Dirac distribution function, the conduction band DOS $D_C(E) = D_{C0}\sqrt{(E - E_C)}$, and

$$p(E) = \left(2\pi\sigma_\phi^2\right)^{-1/2}\int_{E_C}^{E} \exp\left[-(E' - \phi_0)^2/\left(2\sigma_\phi^2\right)\right]dE', \quad (3)$$

as the "percolation factor" running from zero to unity, describing the barrier effect. Furthermore, ϕ_0 is the top of the Gaussian distribution of barriers, and σ_ϕ is its width. It should be noted that, in Ref. 14, the conductivity is taken to be proportional to $(p - p_c)^2$ with p_c as the percolation threshold and 2 as the critical exponent, instead of just to $p(E)$ as in Eq. (2). A more detailed description of the Kamiya-Nomura model is given in Ref. 1 and its supplementary information.

B. Extended mobility edge model

The extended mobility edge model, meanwhile, assumes that, with the presence of sufficiently strong energetic disorder, a tail of localized states can develop below a mobility edge E_C.[15] In order to contribute to the transport, charge carriers need to be thermally excited over the mobility edge. For transistor measurements, the details of these tail states are very important as they determine which portion of the induced accumulation of charge carriers participates in the transport. In a ME model, the charge carriers in the localized tail states are typically assumed to be trapped and immobile. However, Mott showed that transport between localized states is possible by hopping.[10,16] Hopping requires thermal activation to go from low- to high-energy localized states. Whether hopping and/or bandlike transport have a significant contribution to the total current depends on the shape of the DOS, the temperature, and the charge-carrier density.[17] So far, VRH was not considered to be relevant in a-IGZO because of the observation of a well-developed Hall effect.[3,7] However, having bandlike transport above the mobility edge does not exclude VRH below the mobility edge to exist simultaneously.

The eME model applied in this paper allows VRH below E_C to coexist next to the bandlike transport above E_C. The DOS is defined as

$$G(E) \equiv \begin{cases} \frac{n_0}{k_B T_0}\exp\left(-\frac{E}{k_B T_0}\right) & \text{for} \quad E < E_C \\ \frac{n_0}{k_B T_0} & \text{for} \quad E \geqslant E_C \end{cases} \quad (E_C = 0), \quad (4)$$

with n_0 as the density of localized states, T_0 as the width of the exponential tail of localized states, and k_B as the Boltzmann constant. The DOS above E_C is chosen such that the DOS is a continuous function with as few fitting parameters as possible.

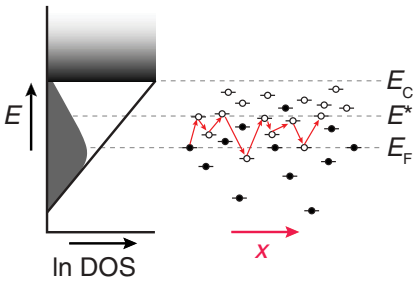

FIG. 3. (Color online) The logarithm of the exponential DOS tail below E_C and the bandlike states above E_C. The cartoon shows the concept of the transport level E^*. The homogeneously gray area indicates occupied localized states around E_F.

Due to the sharp decrease in the Fermi-Dirac distribution above the Fermi level E_F, the conduction is mainly determined by the value of the DOS at E_C. The exact shape of the DOS above E_C is expected to be of minor importance when the Fermi level is below E_C.

The conductivity above the mobility edge is calculated by

$$\sigma_{ME} = e\mu_{free}\int_{E_C}^{\infty} f_{FD}(E)G(E)dE, \quad (5)$$

with the integral being the number of particles above E_C and μ_{free} being the band mobility.

The VRH contribution to the conductivity is described by the Mott-Martens model.[18,19] This model uses a percolation argument with a critical number of hops B_C within a four-dimensional sphere of the typical hopping distance R^* and energy difference between the E_F and an effective transport level E^*,

$$B_C = \frac{4}{3}\pi R^{*3}\int_{E_F}^{E^*} G(E)dE, \quad (6)$$

with $B_C = 2.8$. Figure 3 shows a representation of the DOS and the transport level E^*. The model is based on the assumption that charge transport is limited by a critical hop over an energy $E^* - E_F$ and distance R^* such that the charge carriers have a sufficient number of unoccupied states (B_C) available within the four-dimensional volume set by E^* and R^*. Therefore, E^* and R^* both depend on the temperature and the DOS. With increasing temperature, the increased thermal activation will increase E^* and will decrease R^*; an increased DOS will decrease both E^* and R^*. In the hybrid model presented here, there is the extra constraint that E^* should be smaller than E_C. The VRH conductivity is, subsequently, calculated by optimizing a Miller-Abrahams-type expression,[10,18]

$$\sigma_{VRH} = \sigma_0 \exp[-2\alpha R^* - (E^* - E_F)/(k_B T)], \quad (7)$$

with σ_0 being a conductivity prefactor and α being the inverse decay length of the localized state.

The total conductivity of the extended mobility edge model is a superposition of the VRH conductivity and the band conductivity, viz.,

$$\sigma_{eME} = \sigma_{ME} + \sigma_{VRH}. \quad (8)$$

C. The Seebeck coefficient

In order to calculate the Seebeck coefficient, the energy and the relative contribution to the charge transport of all relevant states have to be known. For the two charge transport models described above, a fit to the transfer curves is sufficient to have all necessary parameters.

From the empirical charge current and heat current relations, and the Onsager reciprocity relations, it follows that the Seebeck coefficient can be written as the Peltier coefficient Π divided by the temperature.[20–22] The Peltier coefficient equals the heat per unit charge that is transported by a charge current. From this, the Seebeck coefficient follows as

$$S = \frac{\Pi}{T} = \frac{\int (E - E_F)\sigma(E)dE}{eT\int \sigma(E)dE}, \tag{9}$$

which is the heat carried by a charge carrier $E - E_F$, weighed by $\sigma(E)/[\int \sigma(E)dE]$, the contribution to the conductivity by the states at energy E.

For the Kamiya-Nomura model, the calculation of S is quite straightforward. Using Eq. (2), $S(E)$ can be calculated as

$$S_{KN} = \frac{\int (E - E_F)p(E)\tau(E)v_z\frac{\partial f_{FD}}{\partial v_z}D_C(E)dE}{eT\int p(E)\tau(E)v_z(E)\frac{\partial f_{FD}}{\partial v_z}D_C(E)dE}. \tag{10}$$

The Seebeck coefficient for the extended mobility edge model is calculated from a contribution from the VRH S_{VRH} and a contribution from the transport above E_C S_{ME}. For S_{ME}, the states below the mobility edge can be ignored, and Eq. (9) reduces to[23]

$$S_{ME} = \frac{(E_C - E_F)}{eT} + A, \tag{11}$$

with

$$A = \int_{E_C}^{\infty}\frac{\varepsilon}{eT}\sigma_{ME}(\varepsilon)d\varepsilon \Big/ \int_{E_C}^{\infty}\sigma_{ME}(\varepsilon)d\varepsilon, \tag{12}$$

where A is the contribution from states above the mobility edge and $\sigma_{ME}(E) = e\mu_{free}f_{FD}(E)G(E)$. In practice, A is relatively small, although it cannot always be ignored altogether.

For the VRH part, where the transport is dominated by the critical hops from the Fermi energy to a narrow region around E^*, the Seebeck coefficient is written as

$$S_{VRH} = \frac{(E^* - E_F)}{eT}. \tag{13}$$

For the total Seebeck coefficient of the extended mobility edge model, Eq. (9) is again used to come to

$$S_{eME} = \frac{S_{ME}\sigma_{ME} + S_{VRH}\sigma_{VRH}}{\sigma_{ME} + \sigma_{VRH}}, \tag{14}$$

i.e., S_{eME} is the conductivity-weighted average of the contributions from localized and delocalized states.

V. EXPERIMENTAL RESULTS AND DISCUSSION

The experimentally determined charge-carrier mobility and Seebeck coefficient of the a-IGZO transistors are plotted in Fig. 4 (symbols) as a function of gate bias for temperatures between 150 and 310 K. The experiments show that mobility increases with temperature and gate bias [Fig. 4(a)]. The Seebeck coefficient reduces with gate bias and is weakly temperature dependent [Fig. 4(b)]. In the following sections, we test the validity of the Kamiya-Nomura and extended mobility edge models for giving a consistent description of these experimental results on a-IGZO.

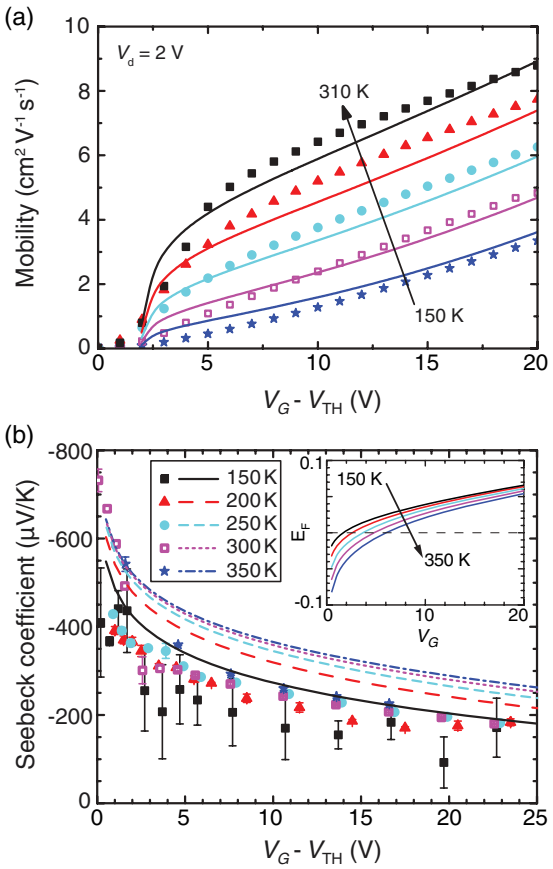

FIG. 4. (Color online) (a) The measured (symbols) and calculated (lines) mobilities vs gate biases for different temperatures. The calculations are performed using the Kamiya-Nomura model and the fit parameters in Table I. (b) The measured (symbols) and calculated (lines) Seebeck coefficients vs gate biases for different temperatures. The inset shows the position of the Fermi level with respect to the band edge (dashed line).

A. The Kamiya-Nomura model

To obtain all the device parameters for the Kamiya-Nomura model, we first extract mobilities from the transfer curves using Eq. (1) and then fit these mobilities with Eq. (2) where we derive the associated mobility by dividing the conductivity by the gate-bias-induced charge-carrier density and the elementary charge. The calculated mobility vs V_G results are shown in Fig. 4(a) together with the experimental results. The curves are calculated using the parameters in Table I. For a TFT with a SiO_2 dielectric, additional trapping states can be present in the SiO_2,[24,25] which could increase the subgap DOS. Nevertheless, the fitting parameters are very much comparable to those found for bulk a-IGZO in Ref. 1.

Without further fitting, the parameters in Table I enable the calculation of the Seebeck coefficient using Eq. (10). The calculated Seebeck coefficients are shown as a function of gate bias and temperature in Fig. 4(b). Compared to the measured

TABLE I. The values of the fit parameters used for the calculations of the Kamiya-Nomura model displayed in Fig. 4.

Fit parameter	Value
D_{C0}	$18 \times 10^{26}\ \mathrm{m^{-3}\ eV^{-3/2}}$
τ	1.02×10^{-15} s
m_e^*	$0.35 \times m_0$
σ_ϕ	0.05 eV
ϕ_0	0.15 eV

data, the calculated values for S are too high, but the curves do show the correct gate bias and temperature dependence and can be regarded as a reasonable prediction of the experiment. The correct gate-bias dependence follows from the increase in E_F with increasing gate bias. With the Fermi level increasing, it approaches the energy of the high-energy states, reducing $E - E_F$ in Eq. (10). Moreover, it should be noted that the determined parameters imply that, for most gate-bias and temperature values, the Fermi level lies in the conduction band ($E_F > E_C$) as shown in the inset of Fig. 4(b).

Predicting the correct temperature dependence from Eq. (10) is not straightforward. When E_F is below a band or in an increasing DOS, E_F increases with decreasing T in order to maintain a constant charge-carrier density. This decreases the term $E - E_F$. However, the denominator in Eq. (10) contains T, which decreases as well. A decrease in S with decreasing T can, therefore, not be intuitively explained on the basis of the above arguments.

Summarizing, the Kamiya-Nomura model gives a good fit to the mobility data with representative fitting parameters. These give rise to a reasonable prediction of the Seebeck coefficient. The calculations give a Fermi level that lies in the band of mobile states, which is chosen to have a square-root dependence on the energy. In the next section, we will use a SKPM technique to measure the DOS shape at the Fermi level.

B. Determining the DOS using a Kelvin probe

In any transport model, the DOS is a key ingredient. Consequently, when a transport model is assumed, information regarding the DOS can be extracted by fitting to transport measurements as in the previous section where the characteristic parameters of a fixed DOS shape are fitted. For some transport models, it is possible to extract the entire DOS from transport data without any *a priori* assumptions regarding the DOS shape. This was, for instance, performed by Chen *et al.* for a-IGZO.[26] However, for the present purposes of finding the actual transport mechanism, this method cannot be used, and the DOS should be determined by independent means.

Previously, Park *et al.* used capacitance-voltage- (C-V)-based methods to extract the DOS in different a-IGZO samples and found either a combination of an exponential and a Gaussian[8] or, from a remarkably similar dataset, a tail of two exponentials.[8,9] Such exponential tails seem reasonable in view of the Anderson localization model for disordered materials.[15]

In this section, we measure the DOS of an a-IGZO TFT, using the scanning Kelvin probe microscopy technique described in Refs. 11 and 27. The technique uses a metallic atomic force microscopy (AFM) probe tip to analyze the potential at the a-IGZO surface and is explained in Fig. 5, which displays the band and energy levels for the different layers in the sample. With no electric field present between the gate and the a-IGZO, no charges are accumulated, and the energy levels are represented by the solid black lines. The electric field between the AFM tip and the a-IGZO surface is nullified by applying a potential V_{SKPM} to the tip.

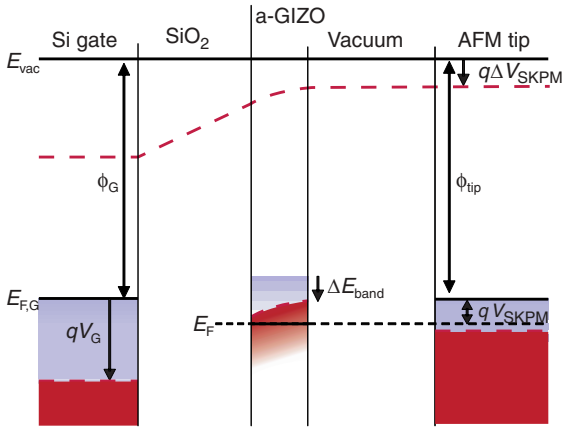

FIG. 5. (Color online) Energy-band diagram of the scanning Kelvin probe experiment used for the DOS extraction. The black solid (red dashed) lines are the levels when no gate bias (a positive gate bias) is applied.

Applying a gate bias V_G with respect to the source and drain electrodes forms an accumulation layer in the a-IGZO. This fills the conduction band, and with the source and drain electrodes fixed at 0 V, E_F does not move and, consequently, the conduction band needs to shift to a lower energy. The shift in the band ΔE_{band} at the sample surface equals ΔV_{SKPM}. Assuming a homogeneous DOS and permeability throughout the IGZO layer, a DOS can be calculated.

For a homogeneous charge-carrier density throughout the semiconductor layer with thickness d_{IGZO}, i.e., in the absence of band bending, the DOS at E_F can be calculated from[27]

$$G(E_F) = \frac{\Delta n(E_F)}{\Delta E_{band}(E_F)} = \left[\left(\frac{dV_{SKPM}}{dV_G}\right)^{-1} - 1\right]\frac{C}{d_{IGZO}q^2}, \tag{15}$$

where C is the areal gate capacitance.

However, the accumulation layer is mainly formed at the SiO_2/a-IGZO interface, and consequently, the band bending displayed in Fig. 5 needs to be taken into account. Unfortunately, no analytical equivalent of Eq. (15) exists, which does account for band bending. We, therefore, use the following procedure to extract G from $V_{SKPM}(V_G)$.

Starting from a trial DOS G_{trial}, one can numerically calculate the change in surface potential vs gate voltage, i.e., $V_{SKPM}(V_G)$. First, the gate voltage sets the total charge density in the channels as $N = \int_0^{d_{IGZO}} n(z)dz = CV_G$. Then, the charge-density distribution $n(z)$ in the channel follows from Poisson's law,

$$\frac{d^2V}{dz^2} = \frac{en(z)}{\varepsilon}, \tag{16}$$

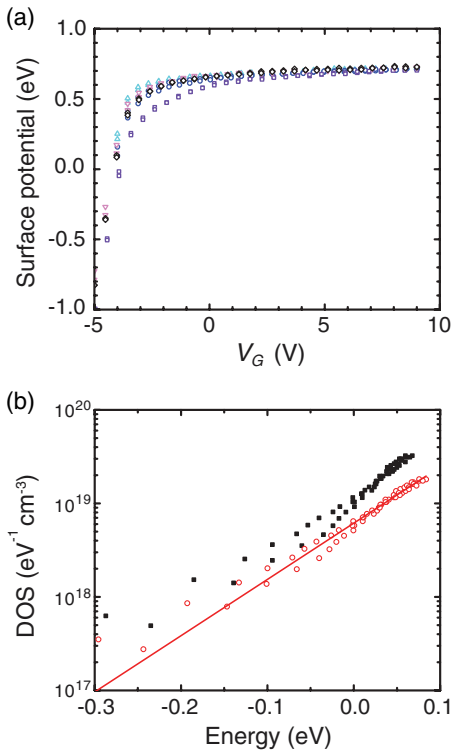

FIG. 6. (Color online) (a) The measured surface potential $q\,\Delta V_{\mathrm{SKPM}}$ vs gate bias at five different locations in the channel of an a-IGZO TFT. (b) The extracted DOS without band bending (black squares) and with band bending taken into account (red circles). The line is an exponential fit through the circles.

using the boundary condition that the derivative of the electric field at the a-IGZO/vacuum interface is zero, which follows from charge neutrality in the entire system. Moreover, for each position in the active layer z, one has

$$n(z) = \int_{-\infty}^{\infty} G\,[E + eV(z)]\,f_{\mathrm{FD}}(z)dE. \tag{17}$$

For each V_G, Eqs. (16) and (17) can be solved by forward integration towards the a-IGZO/vacuum interface. Using Eq. (15) the resulting $V_{\mathrm{SKPM}}(V_G)$ curve can be transformed into an apparent DOS G_{app}. The difference $\Delta G = (G_{\mathrm{app}} - G_{\mathrm{trial}})$ is then taken as a measure for the error that is made by ignoring the band bending in calculating G_{exp} from the experimental $V_{\mathrm{SKPM}}(V_G)$ data with Eq. (15). A new trial DOS is then calculated as $G_{\mathrm{trial}} = G_{\mathrm{exp}} - \Delta G$. This procedure is iterated until self-consistency is obtained and G_{trial} no longer changes. The stable function G_{trial} should then be a good approximation of the real density of states $G(E)$ of the a-IGZO that underlays the band-bending-affected SKPM measurement. In order to stabilize this procedure, G_{trial} is approximated by an analytical expression with a number of free fitting parameters. Internal consistency is assured by validating that the final solution $G(E)$ can indeed be well described by the chosen analytical expression. For the present purposes, it turned out that $G(E)$ can sufficiently be accurately approximated with a single exponential.

TABLE II. Extracted values of the characteristic temperature of the exponential DOS of a-IGZO.

Position	T_0 (K)
1	743
2	836
3	1231
4	758
5	836

Measurements of the surface potentials as a function of gate bias are shown in Fig. 6(a) for five different locations in the channel of an a-IGZO TFT; an example of the derived DOS is shown in Fig. 6(b). The black squares are calculated directly with Eq. (15), i.e., by ignoring band bending, the circles show the final result of the iterative procedure described above, i.e., including band bending, and the line is an exponential fit. The characteristic temperature T_0 of the exponential DOS,

$$G\,(E) \propto \exp\left(-\frac{E}{k_{\mathrm{B}}T_0}\right) \tag{18}$$

is given in Table II. From these measurements, we conclude that, under the operational conditions employed here, the Fermi level E_{F} lies in an exponential tail of the a-IGZO DOS with $T_0 \approx 800$ K.

The obtained exponential DOS is inconsistent with the fitting result of the Kamiya-Nomura model in the previous subsection, where the fitting parameters imply that E_{F} lies in a band with an algebraic (square-root) energy dependence. A tail of localized states was also shown by Kamiya *et al.*[28] but was assumed to be very small. In principle, incorporating the measured exponential tail states in the Kamiya-Nomura model is possible. However, this would lead to a model that is essentially equivalent to the eME model but with a far more complicated contribution of the band states due to the additional Gaussian distribution of barriers. Moreover, the largely increased number of free parameters would make such a model underdetermined. In the following section, the obtained DOS is, therefore, used in the extended mobility edge model.

C. Extended mobility edge model

For the eME model, we use the DOS measurements in the previous subsection, which yielded $T_0 = 800$ K for the exponential tail of the DOS in Eq. (4). For consistency with the DOS measurement analysis, band bending was included in the eME model by treating the channel as parallel quasi-two-dimensional sheets of which the densities are calculated as described at Eqs. (16) and (17). The measured and the fitted mobility data are shown in Fig. 7(a); the corresponding parameters are given in Table III. The fit does not reflect the strong onset of the high-temperature mobility as clearly as the Kamiya-Nomura model. The overall curvature by the Kamiya-Nomura model seems somewhat better, but the calculated eME model values still provide a rather accurate description of the measured values. Using the parameters obtained in the mobility fitting, the Seebeck coefficient is calculated from Eqs. (11)–(14). Both measurements and calculations

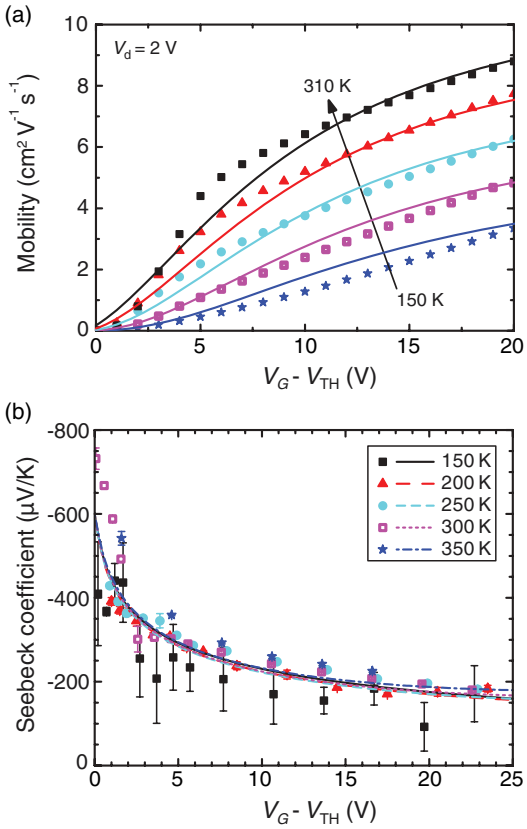

FIG. 7. (Color online) The measured (symbols) and the calculated (lines) (a) mobilities and (b) Seebeck coefficients vs gate biases for different temperatures. The calculations are performed using the eME model and the parameters in Table III.

are shown in Fig. 7(b). The Seebeck coefficient calculations show very good agreement with the experiments. They show the correct gate-bias dependence, and the calculated small temperature dependence of the Seebeck coefficient agrees very well with the experiments. Only for low temperatures, do the experimental values show somewhat stronger temperature dependences than the calculated curves. The origin of the gate bias and temperature dependence follows from the same line of argument as in the discussion in Sec. IV A on the Kamiya-Nomura model.

Comparing the results from the Kamiya-Nomura model with the extended mobility edge model shows that the eME model gives a better description of the experimental Seebeck results. Furthermore, the eME is consistent with the DOS measurement, which shows that E_F lies in an exponential DOS.

The value obtained for the localization length $\alpha^{-1} = 4.8$ nm may appear surprisingly large, given that vacuum tunneling

TABLE III. Device parameters used for the calculations of the eME model displayed in Fig. 7.

T_0	800 K
σ_0	4.6×10^4 S m^{-1}
α^{-1}	4.8×10^{-9} m
μ_{ME}	78 cm^2 V^{-1} s^{-1}
n_0	3.4×10^{19} cm^3

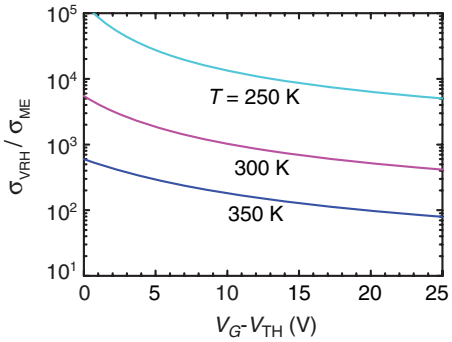

FIG. 8. (Color online) The ratio of the conduction by VRH and the conduction by bandlike transport above E_C for the extended mobility edge model calculations.

typically leads to values around 0.5 nm. However, it seems likely that the tunneling electrons use virtual states in the nearby conduction band ($E_F - E_C \approx 0.3 - 0.6$ eV for the parameters used), which leads to a significant enhancement in α^{-1}.

On further inspection of the calculated results, the contribution of hopping to the conductivity appears to be much larger than the contribution of bandlike transport above the mobility edge. In Fig. 8, the ratio between the two conductivities is shown for three temperatures. The contribution by bandlike transport is on the order of 1%, at most, but usually is much less. However, we were reluctant to use a hopping-only model in view of the observed Hall effect.[1,3] We should note that the values used are the best (mobility) fitting values, but there is definitely room to increase the contribution of the bandlike conduction above E_C while still having a description of the experiments within the error margins. Furthermore, Ref. 1 mentioned the presence of localized states as an explanation for odd charge-carrier density results obtained from Hall measurements. In that paper, the coexistence of hopping and bandlike transport was not considered, and hopping transport was discarded. However, when disallowing hopping conduction in the eME model by setting $\sigma_0 = 0$ S/m, the constraint of $T_0 \approx 800$ K results in extremely poor fits to the mobility curves—actually, an opposite curvature of the gate-voltage dependence is found. Note that this constraint turns the extended ME model into a pure ME model.

Finally, we should note that it is likely that the SiO_2 dielectric causes additional trap states in a-IGZO TFTs, which are absent in bulk a-IGZO devices. These states would lead to an increased contribution of hopping-type transport relative to the bandlike transport in TFT devices. However, our results show that hopping transport cannot up front be ruled out when interpreting the charge transport in amorphous oxide semiconductors.

VI. CONCLUSIONS

We combined three different experiments to investigate the charge transport mechanism in a-IGZO TFTs: an SKPM-based technique to measure the DOS, transfer curve measurements, and Seebeck coefficient measurements. We found that an extended mobility edge model that includes variable range

hopping below the mobility edge gives a consistent and accurate description of the temperature- and gate-voltage-dependent mobility and Seebeck coefficient. The extended mobility edge model is consistent with the Fermi level lying in an exponential DOS with a width of $T_0 = 800$ K, which follows from the DOS measurements.

The calculations show that the contribution of the variable range hopping to the overall charge transport is larger than that of the bandlike transport above the mobility edge.

ACKNOWLEDGMENTS

The work of W.C.G. and M.K. is supported by the Dutch Technology Foundation STW, which is the applied science division of NWO, and the Technology Programme of the Ministry of Economic Affairs (VIDI Grant No. 07575). The research leading to these results has received funding from the European Community's Seventh Framework Program (FP7/2007-2013) under Grant Agreement No. 246334-2 of the ORAMA Project.

*Corresponding author: m.kemerink@tue.nl

[1] T. Kamiya, K. Nomura, and H. Hosono, Appl. Phys. Lett. **96**, 122103 (2010).

[2] M. Kimura, T. Kamiya, T. Nakanishi, K. Nomura, and H. Hosono, Appl. Phys. Lett. **96**, 262105 (2010).

[3] A. Takagi, K. Nomura, H. Ohta, H. Yanagi, T. Kamiya, M. Hirano, and H. Hosono, Thin Solid Films **486**, 38 (2005).

[4] J.-H. Park, K. Jeon, S. Lee, S. Kim, S. Kim, I. Song, J. Park, Y. Park, C. J. Kim, D. M. Kim, and D. H. Kim, J. Electrochem. Soc. **157**, H272 (2010).

[5] S. Lee, S. Park, S. Kim, Y. Jeon, K. Jeon, J.-H. Park, J. Park, I. Song, C. J. Kim, Y. Park, D. M. Kim, and D. H. Kim, IEEE Electron Device Lett. **31**, 231 (2010).

[6] K. Nomura, H. Ohta, A. Takagi, T. Kamiya, M. Hirano, and H. Hosono, Nature (London) **432**, 488 (2004).

[7] T. Kamiya, K. Nomura, and H. Hosono, Sci. Technol. Adv. Mater. **11**, 044305 (2010).

[8] J. Park, K. Jeon, S. Lee, S. Kim, S. Kim, I. Song, C. J. Kim, J. Park, Y. Park, D. M. Kim, and D. H. Kim, IEEE Electron Device Lett. **29**, 1292 (2008).

[9] K. Jeon, C. Kim, I. Song, J. Park, S. Kim, S. Kim, Y. Park, J. Park, S. Lee, D. M. Kim, and D. H. Kim, Appl. Phys. Lett. **93**, 182102 (2008).

[10] N. F. Mott and E. A. Davis, *Electronic Processes in Non-Crystalline Materials*, 2nd ed. (Oxford University Press, Oxford, 1979).

[11] W. S. C. Roelofs, S. G. J. Mathijssen, R. A. J. Janssen, D. M. de Leeuw, and M. Kemerink, Phys. Rev. B **85**, 085202 (2012).

[12] A. K. Tripathi, E. C. P. Smits, J. B. P. H. van der Putten, M. van Neer, K. Myny, M. Nag, S. Steudel, P. Vicca, K. O'Neill, E. van Veenendaal, J. Genoe, P. Heremans, and G. H. Gelinck, Appl. Phys. Lett. **98**, 162102 (2011).

[13] J. S. Dugdale, *The Electrical Properties of Metals and Alloys* (Arnold, London, 1977).

[14] D. Adler, L. P. Flora, and S. D. Senturia, Solid State Commun. **12**, 9 (1973).

[15] P. W. Anderson, Phys. Rev. **109**, 1492 (1958).

[16] N. F. Mott, J. Phys. C **20**, 3075 (1987).

[17] W. C. Germs, K. Guo, R. A. J. Janssen, and M. Kemerink, Phys. Rev. Lett. **109**, 016601 (2012).

[18] H. C. F. Martens, I. N. Hulea, I. Romijn, H. B. Brom, W. F. Pasveer, and M. A. J. Michels, Phys. Rev. B **67**, 121203 (2003).

[19] R. Coehoorn, W. F. Pasveer, P. A. Bobbert, and M. A. J. Michels, Phys. Rev. B **72**, 155206 (2005).

[20] R. G. Chambers, Phys. Educ. **12**, 347 (1977).

[21] L. Onsager, Phys. Rev. **37**, 405 (1931).

[22] R. E. Bentley, *Handbook of Temperature Measurement: Theory and Practice of Thermoelectric Thermometry* (Springer-Verlag, Singapore, 1998), Vol. 3.

[23] H. Fritzsche, Solid State Commun. **9**, 1813 (1971).

[24] J. Veres, S. Ogier, G. Lloyd, and D. de Leeuw, Chem. Mater. **16**, 4543 (2004).

[25] A. Sharma, N. M. A. Janssen, S. G. J. Mathijssen, D. M. de Leeuw, M. Kemerink, and P. A. Bobbert, Phys. Rev. B **83**, 125310 (2011).

[26] C. Chen, K. Abe, H. Kumomi, and J. Kanicki, IEEE Trans. Electron Devices **56**, 1177 (2009).

[27] O. Tal, Y. Rosenwaks, Y. Preezant, N. Tessler, C. K. Chan, and A. Kahn, Phys. Rev. Lett. **95**, 256405 (2005).

[28] T. Kamiya, K. Nomura, and H. Hosono, J. Disp. Technol. **5**, 273 (2009).